Nanostructured surfaces described by atomistic simulation methods

2003 J. Phys.: Condens. Matter 15 S3153

(http://iopscience.iop.org/0953-8984/15/42/012)

INSTITUTE OF PHYSICS PUBLISHING JOURNAL OF PHYSICS: CONDENSED MATTER

J. Phys.: Condens. Matter **15** (2003) S3153–S3169 PII: S0953-8984(03)61184-7

Nanostructured surfaces described by atomistic simulation methods

Roger Smith[1], **S D Kenny**[1], **C F Sanz-Navarro**[1] **and Joseph J Belbruno**[2]

[1] Department of Mathematical Sciences, Loughborough University, Leicestershire LE11 3TU, UK
[2] Department of Chemistry, Dartmouth College, Hanover, NH 03755, USA

E-mail: r.smith@lboro.ac.uk

Received 21 March 2003
Published 10 October 2003
Online at stacks.iop.org/JPhysCM/15/S3153

Abstract

Three separate simulation techniques have been applied to study different problems involving nanostructured surfaces. In the first investigation the bonding of fullerene molecules on silicon and Ag adatoms and dimers on graphite are investigated using the PLATO density functional code. It is shown that in the first case there are strong covalent bonds formed whereas in the latter there are relatively weak bonds with small energy barriers between adjacent sites. Classical MD is used to show how energetic (≈keV) Ag clusters can be pinned on or implanted into a graphite surface and that the pinning thresholds and implantation depths agree with experiment. Finally a Monte Carlo model for cluster motion over a surface is described and related to pattern formation in the early stages of thin film growth.

(Some figures in this article are in colour only in the electronic version)

1. Introduction

The advent of modern high speed computers with visualization capabilities has meant that the formation of nanoscale morphology or the arrangements of atoms and molecules on surfaces can be routinely described by mathematical models of varying degrees of sophistication. Unfortunately because of the complexity of the problems, there is not one overall technique that can be used to describe all length and timescales. The definition of the nanoscale is not completely precise and can be thought of as a region spreading from a few ångströms up to tens or even hundreds of nanometres. Whilst this might not seem a big difference compared to the scale of the universe, from the point of view of computer simulation it is immense. Over this spread of length scales, atomistic simulations can involve calculations involving less than a hundred atoms up to several billion and the same level of detail cannot normally be used to describe both cases. A similar problem involves timescales. Collisional atomic processes

and processes where bonds are formed take place over picosecond timescales. In a computer simulation a typical time step used to integrate the equations is of the order of a femtosecond [1]. However, diffusion processes on surfaces take place over a timescale that can run from fractions of a second to several days. To model a dynamical process involving picoseconds, such as the ballistic phase of a collision cascade or ballistic sputtering using classical potentials is entirely feasible and much work has been done on this problem. However, a diffusional process lasting 1 s would require integrating the equations of motion through $\approx 10^{15}$ time steps, which is clearly unfeasible for any reasonably sized system. Nanostructured surfaces are produced in different ways involving processes that span these timescales. For example, low energy charged particle or cluster beams can be used either to shape morphology or to deposit material. These ballistic processes lend themselves relatively straightforwardly to classical molecular dynamics simulations. If, on the other hand, complex molecules are evaporated onto a surface the dynamics of how the bonding occurs cannot generally be so straightforwardly simulated because both diffusion (long timescales) and surface chemistry (expensive quantum calculations) are involved. Where bonding needs detailed analysis, computer simulations are generally static in nature and restricted to identifying the bonding sites and the surface electronic structure which can be determined by quantum calculations of one form or another. Dynamic quantum calculations are in principle feasible but are computationally very expensive. Both these approaches will be described here with reference to some model systems.

The problem of how to tackle long timescale dynamics is still an area of ongoing research [2, 3]. Various methods have been proposed such as hyper molecular dynamics, parallel replica MD and temperature-accelerated dynamics. All these methods have their problems and long timescale phenomena are not at present analysed with anything like the detail of the short timescale phenomena. The main problem is to determine the transitions and their frequency from one fairly stable system state to another. If a suitable set of transitions can be found then these can be incorporated into a kinetic Monte Carlo (KMC) simulation [4] where time is only included stochastically. In this case the simulation is event driven and time is not specifically included. To obtain all feasible transitions is very difficult and many KMC simulations can omit basic phenomena if they use an incomplete transition set.

In this paper we will describe some recent results involving quantum, classical and stochastic simulations which can be used to understand how some nanostructured surfaces can be formed. The quantum simulations have been carried out using the PLATO code [5, 6] and the classical simulations have been performed using our own in-house MD code. Finally some results will be presented using a simple KMC model [7] that describes the surface patterns that can form as species diffuse and aggregate across a surface.

2. Static calculations using PLATO

PLATO is a density functional theory code in which the Kohn–Sham eigenvectors are expanded in numeric atomic-like orbitals with a finite range [5, 6]. Electron–ion interactions are represented by the pseudopotentials [8] and the exchange correlation potential is taken to be the local density approximation from [9]. The integrals for orbital overlap, kinetic energy, one- and two-centre neutral potential terms, non-local pseudopotential and ion–ion interactions are calculated and tabulated prior to use and interpolated during a calculation. The remaining integrals are calculated numerically on an atom-centred mesh. Forces are obtained using the Hellman–Feynman theorem by differentiation of the total energy and include the contributions from Pulay corrections. More details of the method and its implementation are given in the references. The use of finite-ranged atomic-like orbitals can yield high quality results with relatively small basis sets [6]. The orbitals are forced to go to zero at a selected cut-off radius

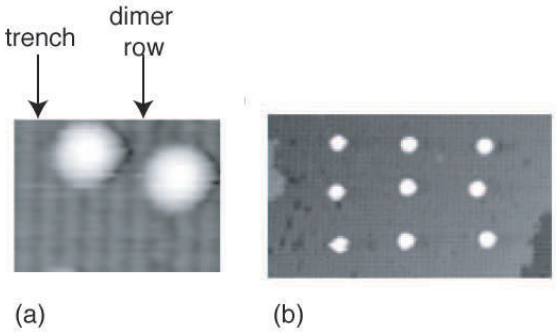

Figure 1. (a) Image of two C_{60} molecules deposited on a clean Si{100} surface; (b) an ordered array of C_{60} molecules after manipulation by an STM tip; figure courtesy of Dr P Moriarty, Nottingham University [12].

which greatly enhances the efficiency of the computational method. PLATO is especially useful for problems involving nanostructured surfaces and to illustrate its applicability we perform calculations which are specific to such surfaces. In the first application C_{60} molecules on Si(100) are used as the basis for a possible future quantum computer [10, 11]. The molecules can be manipulated over the surface using an STM tip to form ordered arrays as shown in figure 1. Thus an understanding of the electronic structure, stable bonding sites and the energy barriers to motion is important. In the second example the application of PLATO is associated with the problem of size-selected Ag clusters being pinned to the surface or implanted below the surface of graphite by direct impact. In this case it is not so easy to manipulate the clusters as they are highly mobile once they detach from their pinning site. Here PLATO is used to obtain knowledge about bonding sites of individual atoms and the energy barriers between sites. The code can be used also to obtain parameters for potentials used in a larger classical MD study.

2.1. The bonding of C_{60} to Si{100}(2×1)

The simulation cell that we used to describe isolated fullerenes on Si(100) consisted of six Si layers with the surface containing two rows of four dimers. The bottom two layers of the silicon were frozen in their bulk positions with the bottom layer terminated with hydrogen. Periodic boundary conditions were imposed in all three directions with a vacuum layer larger than 1.9 nm between the top of the C_{60} molecule and the bottom of the silicon slab. The calculations were carried out using the Γ point for k-point sampling of the Kohn–Sham eigenstates due to the size of the system. We used basis sets containing two s and p type functions and one d type function for both the Si and C atoms, leading to 13 basis functions on each atom. The H atoms are described using a single s function, as the aim is not to provide an accurate description of the H atoms but to saturate the silicon dangling bonds. All calculations were performed using a spin polarized formalism.

Our results indicate that bonding sites exist both in the trench between the dimer rows (most stable) and also on top of the dimer rows (least stable). This is in agreement with the experimental STM results obtained at the University of Nottingham shown in figure 1(a). Figure 1(b) shows how such molecules can be manipulated by the STM tip to form an ordered array on the surface. Molecules bonded to the top of the dimer rows can occasionally be found but only after heating the surface. The theoretical results show covalent bonding between

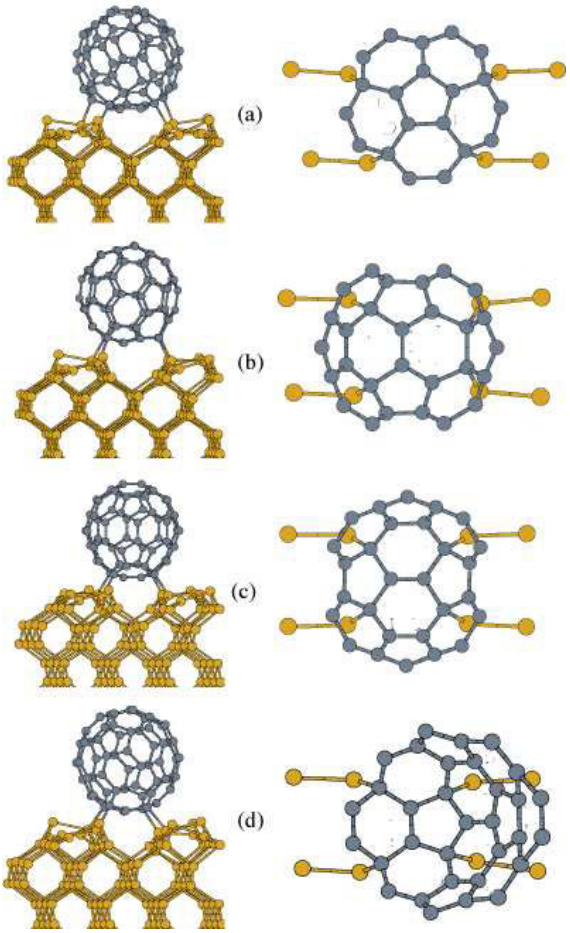

Figure 2. The C_{60} molecule bonded to the most favourable sites on the Si{100} surface with the fullerene over the dimer trench centred between four dimers. Left-hand side: side view; right-hand side: top view showing only the lowest atoms in the C_{60} molecule.

the silicon dimers and the C atoms in the cage of the fullerene in all cases. The C–Si bond lengths lie between about 1.95 and 1.98 Å, which is ≈0.1 Å longer than in SiC. Mulliken population analysis shows only a small charge on the atoms in the bonds, with at most 0.1 electrons transferred onto the C atom. For the C_{60} in the trench, see figure 2, there are unpaired electrons on the silicon dimer atoms at the opposite end to which the C_{60} is bonded. In the C_{60} molecule we see no significant spin with Mulliken spin analysis. However, there is significant rebonding taking place within the molecule.

As is well known there are two types of carbon–carbon bonds alternating in isolated C_{60}. The shorter bond, between adjacent hexagons, can be thought of as a double bond, while the longer bond is between adjacent hexagons and pentagons and corresponds to a single bond. In the isolated C_{60}, these bond lengths are calculated to be 1.39 and 1.44 Å, respectively. The carbon atoms to which the silicon atoms bond were originally double-bonded to one of their neighbours. This π bond is broken, but dangling bonds within the fullerene molecule are absorbed by rebonding taking place within the fullerene molecule. This can clearly be observed both through changes in the bond lengths and the bond energies of these bonds.

A detailed analysis of how rebonding takes place and why the configurations occur as they do is given in [11].

Although a large number of bonding sites are possible both in the trench between the surface dimers and on the dimer row, only the most stable configurations are shown in figure 2. These occur when the molecule lies in the dimer trench bonded to four dimers. Structure (a) has the greatest binding energy, −5.71 eV. Structures (b), (c) and (d) have binding energies of −5.31, −4.96 and −4.85 eV, respectively. These energies are relatively high and it might be expected that the molecules would not be so easily manipulated by the STM tip. Although we have not performed a detailed investigation there is some evidence from the calculations to suggest that motion can occur by rolling within the trench where two bonds break on one side of the molecule at the same time as two others form on the other.

2.2. Ag adatoms and dimers on graphite

In this section we analyse the bonding of Ag adatoms and dimers to graphite [13, 14]. This system is investigated because silver clusters deposited on graphite have been used in complementary experimental work by our collaborators at Birmingham University as a model system for the study of nanostructured surfaces. The investigation of the bonding of large clusters on or their energetic interaction with graphite using PLATO is not yet feasible due to constraints on computer time. Such interactions will be discussed later using classical MD. However, the smaller systems studied using PLATO can be used for the parametrization of the classical potentials used for investigation of the larger systems.

Graphite is a layered structure which has strong covalent bonds between atoms in the layers and weak van der Waals interactions between layers. These two regimes together are not especially easy to handle with density functional theory and relatively large orbital cut-off radii of 7.0 au for carbon and 8.0 au for silver were found to be necessary (1 au = 0.529 Å). Smaller cut-off radii gave too large a value for the contraction between the first and second layers compared to experiment. With the longer cut-off, the calculated contraction of 0.07 Å is highly comparable to the experimental value of 0.05 Å. For the Ag atoms we have used a basis set containing two s and d type orbitals and one p type orbital, the basis set thus containing 15 basis functions.

PLATO uses periodic boundary conditions in the calculations and so equivalent supercells with in-plane sizes of 2×2, 3×3 and 10×10 were tested on silver adatoms and dimers, without the graphite surface, to determine an optimum size. The optimum supercell was set to contain $3 \times 3 \times 2$ primitive cells of graphite with four atomic layers. A vacuum region was set up with half the thickness of the slab, above the surface and below the base layer. The bottom two layers of atoms were fixed, while the top two layers were allowed to relax. The entire graphite system consisted of 72 carbon atoms. Once the graphite surface is relaxed, a silver atom is added above the surface at different binding sites and the system further relaxed. Results show that β sites are preferred for single silver atoms, but the differences in binding energy between various sites are not significant. The energy difference between the β site and the over-hole (OH) site, the least well bound of the binding sites, is only 0.05 eV. This indicates that the energy landscape for the Ag adatom on the graphite surface is very small. The distance between the surface and second layers at the adatom site changes slightly and the closest atom below the silver atom is dragged slightly out of the surface. The calculations also illustrate the necessity of describing a number of layers of graphite in order to correctly calculate adhesion energies.

The energy barriers have not been specifically calculated but we have calculated the binding energy of the Ag adatom at various points along the path between α and β sites along the $\langle 110 \rangle$

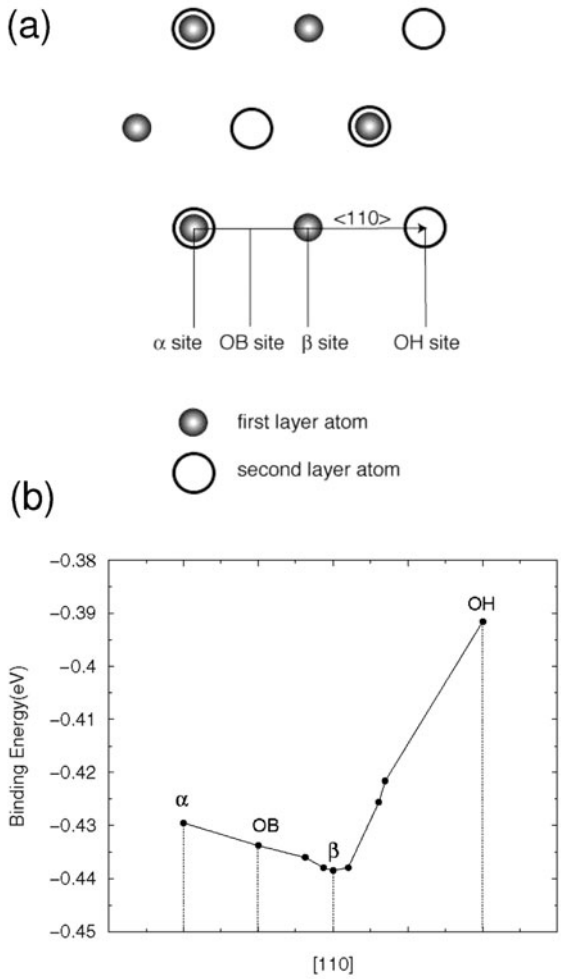

Figure 3. (a) Layout of a graphite surface together with a description of the bonding sites considered for the adatom; (b) the binding energy of the adatom as a function of the sites described in (a).

Table 1. The interactions between a silver adatom and the graphite surface using PLATO with a $3 \times 3 \times 2$ supercell.

Site	E_B (eV)	h_{Ag} (Å)	Δh_C (Å)
α	0.430	2.543	0.046
β	0.439	2.539	0.050
Over-bond (OB)	0.434	2.544	0.038
Over-hole (OH)	0.392	2.613	0.002

direction. This is shown in figure 3 together with the layout of atoms in the surface. Along this path there are low energy differences. Such low barriers are an indication that diffusion of the adatoms over the surface would occur. STM observations [19] show that single silver atoms are visible near β sites only for a brief observation time and move until they are stabilized by a large island, a particle, a defect or the edge of the substrate. Figure 3(b) shows that the binding

energies around the β site are asymmetrical. Since a carbon–carbon bond lies between two holes, the bottom of the well is a deep valley in three dimensions. This suggests that silver atoms would be constrained to move preferentially along the bond and motion towards the holes is unlikely.

Table 1 gives the main features of the calculation in terms of the binding energy of the atatom to the surface (E_B), the height of the adatom above the surface (h_{Ag}) and the protrusion of the nearest C atom above the surface (Δh_C).

The code can also be used to determine the binding energies of Ag_2 dimers. Seven different sites were chosen to be investigated and the surface and dimer relaxed on each occasion. The sites chosen included the centre of the dimer situated above the α and β sites and also above holes and bonds. The binding energy of the dimer to the surface varied by only 0.04 eV at these different sites (marginally less than the Ag adatom) and the dimer bond length varied from 2.58 to 2.60 Å. This compares to a calculated value of 2.53 Å for the free dimer. Thus it would be expected that the dimer would be mobile over the surface and would also diffuse freely at room temperature.

3. Pinning and implantation of size-selected Ag clusters in graphite surfaces using classical MD

3.1. MD methodology

The geometrical arrangement of a free Ag cluster was found by applying a genetic algorithm [15] to a family of random spatial configurations of Ag atoms, interacting with each other through a many-body potential function parametrized by Ackland *et al* [16]. This algorithm is capable of determining minima in structures containing several hundred atoms but the results here are limited to 7 and 147 atoms that are especially stable and have icosahedral symmetry. This same potential was employed during the impact simulations. The cluster was placed above the substrate outside the potential interaction range with zero internal kinetic energy before impact. In most cases the substrate area was taken as 50 Å $\times$ 50 Å and the total number of graphite layers was between 10 and 16, depending on the impact velocity v_0. The covalent C–C interaction was modelled by a many-body Brenner [17, 18] potential while an additional long-range Lennard-Jones potential [19] between atoms that are not linked by covalent bonds was employed to take into account the van der Waals interaction between graphite layers. The carbon atoms at the edges were fixed and adjacent atoms undergo a damped force to prevent lattice displacement waves reflecting back into the impact zone. The Ag–C interaction was modelled in the system by a Morse potential [20], which produces a fair representation of STM results for the adsorption of Ag atoms and clusters on the graphite surface. In addition, we splined the Ag–C potential to the two-body ZBL screened Coulomb potential [21] for high interaction energies. The ZBL potential has been shown to give good agreement with *ab initio* calculations and is fitted to large quantities of ion implantation data [21]. The whole system was initially heated up by thermostat until equilibration at a temperature of 300 K, but was switched off during the impact simulation to prevent the extraction of energy from the system by the thermostat. Normal incidence was always considered.

3.2. MD calculation of pinning thresholds of Ag clusters and comparison to experiment

Pinning thresholds for clusters on surfaces give an example of where classical MD can give good agreement with experiment and where physical explanations can be deduced from the simulations [22, 23]. The basic idea deduced for the criterion for a cluster to be pinned on

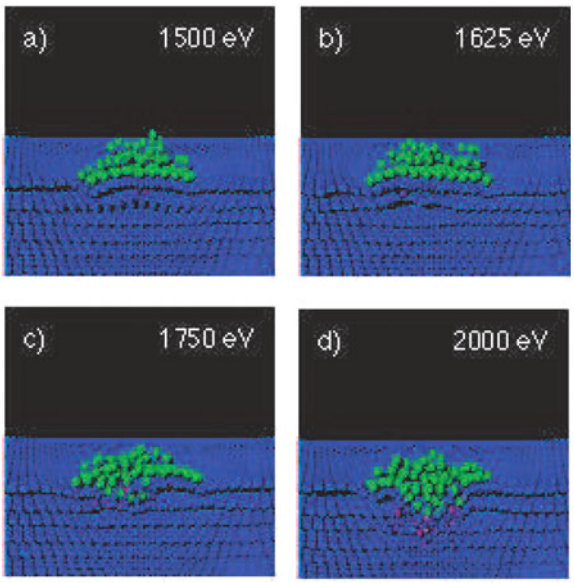

Figure 4. Molecular dynamics simulations, viewed in cross section, of the impact of Ag_{147} at 1500 eV (a), 1625 eV (b), 1750 eV (c) and 2000 eV (d). The cluster impact first creates an atomic defect between 1625 and 1750 eV.

the surface is that its impact energy should be sufficient to permanently displace a graphite atom from its lattice site to form a stable bonding site for the cluster. As an example of the results of the MD simulations, figure 4 shows in cross section what happens when Ag_{147} land on the graphite surface with energies between 1500 and 2000 eV. Because of the very stable geometry, such a cluster would not be expected to break up easily on impact. Below 1625 eV (see figures 4(a) and (b)), the cluster flattens on impact and does not penetrate the surface layer. No silver atoms implant underneath the surface and no carbon atoms are displaced from their lattice sites. As the energy is increased to 1750 eV, figure 4(c), the graphite lattice becomes more disrupted and a few carbon atoms from the surface layer are permanently displaced. As the impact energy of the clusters is increased even further, to 2000 eV, figure 4(d), more of the cluster atoms become implanted. The impact energy for the first permanently displaced C atom, i.e. the pinning threshold for Ag_{147}, would therefore be somewhere between 1625 and 1750 eV, i.e. figures 4(b) and (c). For single-ion impacts the penetration depth and displacement of lattice atoms depends critically on impact site [22, 23]. With clusters this is less significant because averaging plays a role.

The level of agreement between the experimental pinning thresholds obtained from STM experiments and those obtained from the MD simulations is remarkably good, see figure 5. There is a linear dependence of pinning energy with cluster size. Nonetheless the calculated thresholds vary up to 75 eV, depending on the initial orientation of the cluster and the precise impact site [23].

The results also show that the energy per atom corresponding to the onset of pinning is $\approx$10.4 eV/Ag atom. This is substantially less than E_d, the threshold displacement energy of a C atom in graphite ($E_d = 33$ eV from the MD simulations, in agreement with experiment [24]). So a binary collision by a single Ag atom cannot be the mechanism for C atom displacement. If we assume that, at the moment of impact, we have a massive body (the cluster) colliding

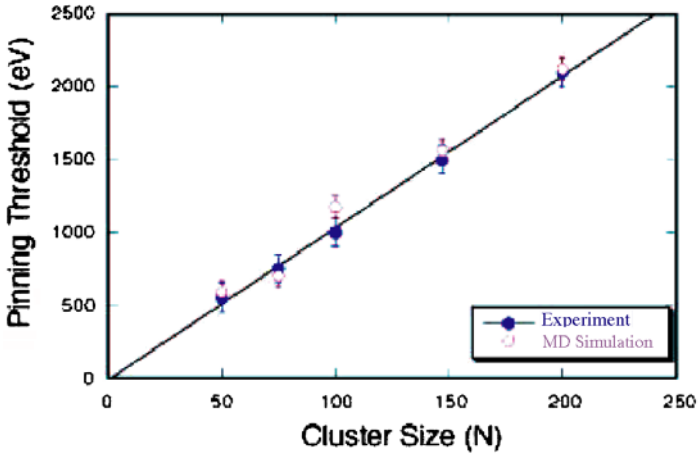

Figure 5. A comparison between MD simulation results and pinning thresholds determined from STM measurements.

with a light body (the recoil carbon atom), then from conservation of energy and momentum for an elastic collision the energy transferred to the recoil carbon atom, E_T, is given by

$$E_T \approx 4\frac{EM_C}{NM_{Ag}}, \tag{1}$$

where E is the impact energy of the cluster and M_C and M_{Ag} are the masses of the carbon and silver atoms, respectively, and N is the number of atoms in the cluster. If we assume that, for pinning to occur, the cluster has to displace a surface carbon atom by providing a critical threshold energy E_C, then pinning will start when $E_T = E_C$. However, assuming a value of $E_C = 33$ eV a value of $N \approx 20$ is obtained. Thus it seems that one cannot assume that the whole cluster acts as a single entity in causing the first atom displacement.

3.3. Implantation depths of an Ag_7 cluster and comparison to experiment

Direct STM observation of the depth of pits produced by implantation of small clusters is not possible since the well diameters, typically of the order 1–2 nm, are much smaller than the diameter of the microscope tip. To investigate these implantation depths Ag_7 clusters were chosen because, as with the larger clusters, these are especially stable and have icosahedral symmetry. Oxidation was used to widen pits formed by the cluster impact followed by an annealing process so the STM tip could be introduced inside in order to measure the depth. The results shown in figure 6(b), the usual annealing temperature, give shallower results compared to MD simulations. Many different effects were analysed to determine the discrepancy, including the consideration of charge on the cluster [25]. However, the discrepancy was discovered to be due to the annealing process with subsurface layers recovering at the higher annealling temperatures [26, 27].

Initially a high temperature was used in the annealing process because the annealing time increases as the temperature decreases. For example, 90 min were necessary when the oxidative etching was carried out at 450 °C, whereas a period of 3 min was enough for etching at the temperature of 650 °C, the normal experimental condition. Such timescales are impossible to simulate using classical MD and so a simulation was run at the higher temperature of 1500 K to enhance the diffusion mechanisms. Figure 7 shows the slow healing process of the third

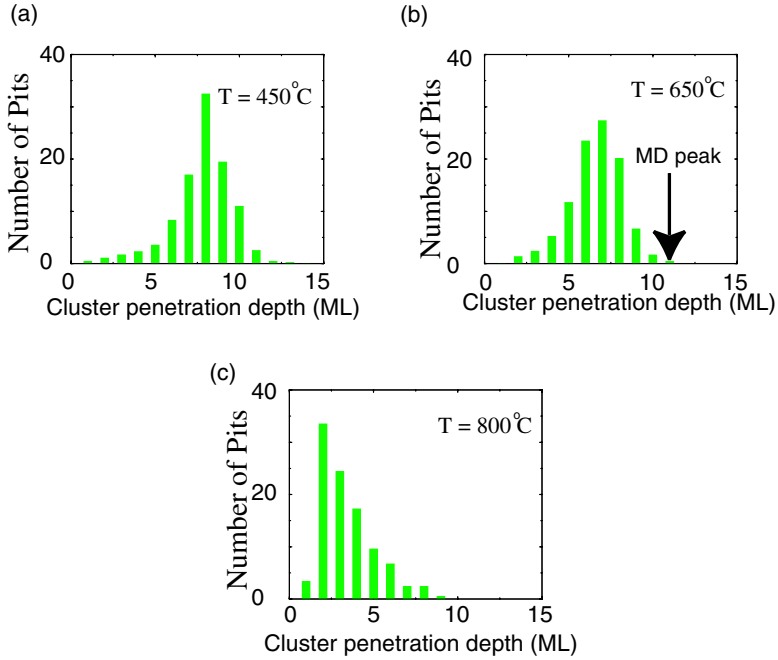

Figure 6. Experimental etch pits depth distributions after A_7^- bombardment at 5 keV followed by (a) oxidative etching at 450 °C for 1.5 h; (b) oxidative etching at 650 °C for 3 min and (c) annealing in UHV at 850 °C for 3 min followed by oxidative etching at the normal temperature of 650 °C. (Figure courtesy of Nanoscale Physics Laboratory, University of Birmingham).

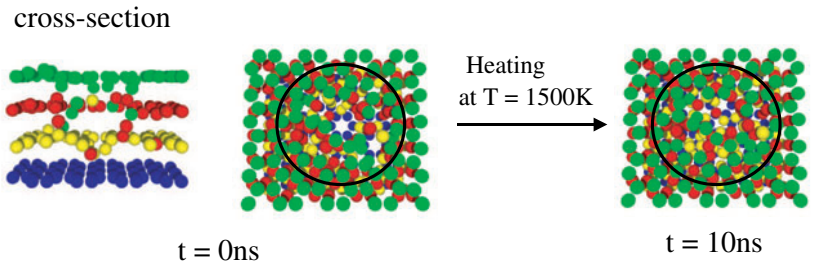

Figure 7. 10 ns MD simulation of annealing of graphite at 1500 K. There is a partial recovery of the third layer of carbon atoms. The silver cluster was removed immediately after impact, so this simulation represents regions of the damaged graphite lattice above the implanted cluster.

layer of a crater opened as a consequence of an Ag_7 impact. A Langevin thermostat kept the system at the desired temperature and provided the canonical ensemble.

In order to obtain an experimental value of the cluster penetration depth much closer to the experimental results at the normal annealing temperature, the STM distributions were fitted to Gaussian functions [28] and then a mean value that corresponds to that part of the distribution that lies two standard deviations deeper than the peak was used. With this correction, excellent agreement with experiment is obtained [26] and a linear dependence of the implantation depth of the Ag_7 cluster on the impact velocity is found. This same behaviour has been extended to Au_7 and Si_7 clusters [29]. This 'universal' behaviour might be exploited to create well-defined nanometre-scale clusters for application in single-molecule science.

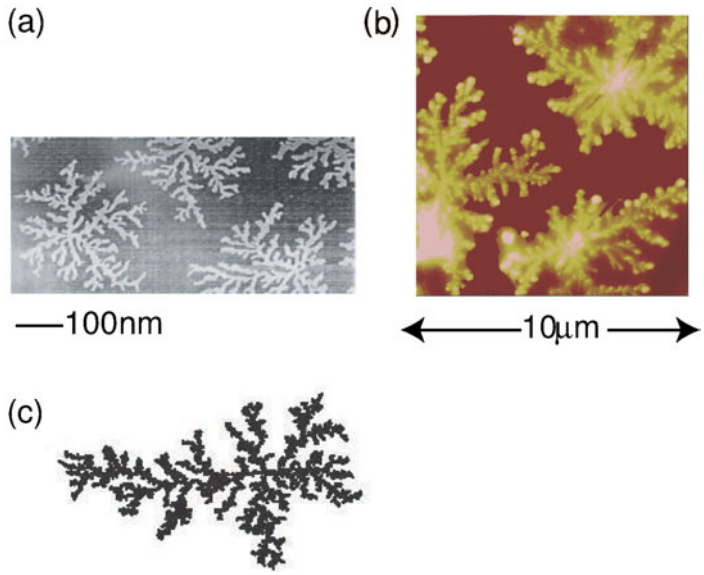

Figure 8. (a) Scanning tunnelling microscopy image of the initial stages of growth of a gold film on Ru{0001} at room temperature. The radius of the fractal islands is between 300 and 400 nm. The flux is approximately 0.2 ML min^{-1}. (b) Scanning force microscopy image of NaCl crystals grown on glass by evaporation of small droplets of brine. (c) Computer simulation of dla on a hexagonal grid.

4. KMC simulations of cluster diffusion over surfaces

In the previous sections nanostructured surfaces involving clusters have arisen as a result of the direct manipulation of molecules using an STM tip or by direct pinning to the surface by a correct choice of deposition energy. In the latter case, when an insufficiently large energy is given to the clusters for pinning to occur, the clusters are highly mobile over the surface and diffusion is the dominant mechanism. This cannot be examined easily using MD because of the long timescale of the diffusion process. For the case of Ag clusters on graphite the clusters aggregate at defects, such as edges and steps, on the surface where they bind the most strongly. Film growth occurs as more clusters are deposited, initiated from these defects. In order to investigate the phenomenon where there are mobile atoms and clusters on a surface which, under the influence of diffusion, organize to form special patterns as the layer grows we develop a Monte Carlo model for the growth on surfaces. It is not possible to use the methodologies described previously as the timescales and system sizes required are prohibitively expensive computationally. The motivation was to develop a simple model to study C_{60} films after the deposition of large numbers of molecules but with sub-monolayer coverage.

The model described here is an adaptation of the diffusion limited aggregation (dla) model for island growth [30]. In the two-dimensional dla model a (usually square) grid representing the surface is defined and a seed particle fixed near the centre of the grid. An incoming particle is initiated by choosing a random point on a circle of a large radius whose centre is taken to be the same as that of the square grid. This particle then undergoes a random walk over the grid until it either reaches the central particle, where it is assumed to stick, or moves outside a circle of a larger radius, whence it is assumed to disappear from the system. The simulation is then repeated with another incoming particle until the shape of the central structure becomes apparent.

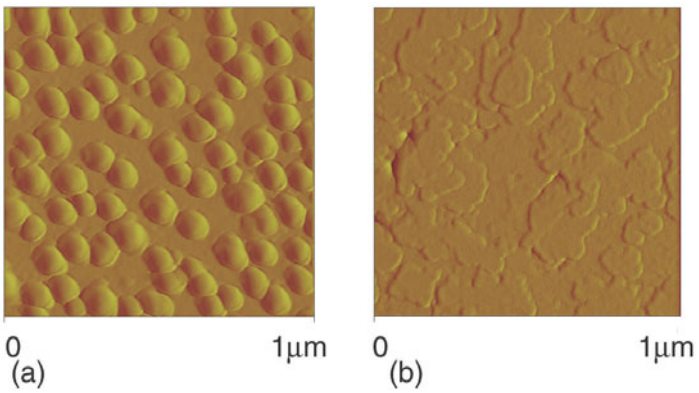

Figure 9. Scanning force microscopy images of C_{60} films grown at a temperature of 250 °C on (a) glass and (b) mica. The average film thickness is 4 nm. Figure courtesy of Professor A Richter, University of Applied Sciences, Wildau, Germany.

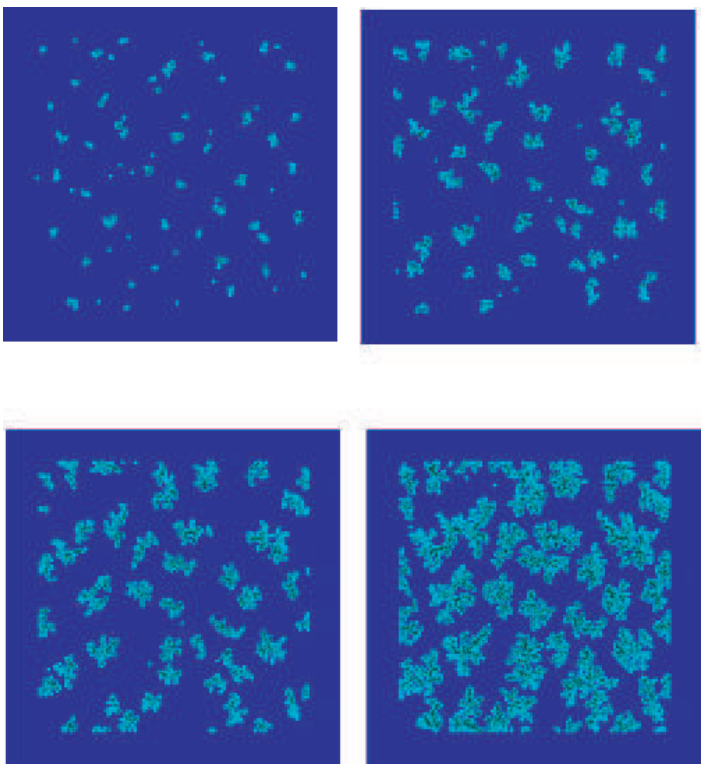

Figure 10. Various stages in the development of thin film growth using the Monte Carlo simulation model with $\alpha = 2$, $E = 0.5$, $R = 1$ and $F = 0.0125$.

The simple dla model results in the typical fractal shapes shown in figure 8(c). The resulting shapes are representative of many growth phenomena seen at surfaces, e.g. the growth of a gold film on Ru{0001} [31] or the formation of NaCl crystals on a glass substrate [32]. Isolated

fractal islands are not so predominant with graphite because edge defects are common and diffusing atoms aggregate there. The corresponding micrographs for this experimental work are shown in figures 8(a) and (b). Other growth processes require more sophisticated models. In the case of Au on Ru{0001} the initial gold seeds are pinned at defects in the ruthenium surface and therefore the resulting fractal islands that form are immobile. In addition, although the gold atoms are mobile over the ruthenium surface, there is a strong binding of the Au particles to themselves.

In the case of fullerene films grown on different substrates by evaporation [7, 33]. Fullerene clusters can form on the surface but there is more mobility of the fullerene particles within these cluster islands. In addition, before the islands grow too large in size, they themselves are mobile. There are therefore three competing effects: the rate of arrival of molecules on the surface, the rate of diffusion of the fullerene clusters over the surface and the rate of diffusion of the molecules within each cluster. It could also be the case that the clusters can themselves dissociate but this is not included in the model described below.

(1) The substrate material is represented by a hexagonal grid of cells. All the simulations were conducted on a square 400×400 lattice with periodic boundary conditions.
(2) The simulation is two-dimensional only. Particles arrive randomly on the surface and undertake random walks over the surface until they reach an edge between filled and unfilled sites. If an incoming particle lands on a filled site, this could also include walks over filled sites until the edge is reached.
(3) Clusters are defined to be linked sets of filled cells which are separated from other filled cells by unfilled regions. Clusters also move over the surface but if they coalesce with another cluster then the result is assumed to be a single cluster. Single clusters are not allowed to divide into smaller clusters.
(4) At each step in the simulation either a new particle arrives on the surface, depending on the arrival probability F, or an existing particle or cluster diffuses over the surface. The diffusion probability P_D of a cluster is assumed to depend on the number of particles N in the cluster. We have chosen a power law dependence $P_D = N^{-\alpha}$. Here α is a variable parameter which controls the relative diffusion of clusters of different sizes. Thus, if N and α are large the clusters have a small probability of motion. If α is near zero then all clusters move at similar speeds.
(5) The model for diffusion within a cluster is as follows. Particles are randomly selected in a cluster and allowed to move to adjacent sites within a fixed radius R of the existing site according to the following rules.
    (a) Vacant sites within a circle of radius R are examined to see how many adjacent filled sites they have. (This is a number between 1 and 6.)
    (b) Vacant sites with the largest number N_n of filled neighbours are chosen as possible candidates for the new position. If more than one site has N_n neighbours then the site chosen is that nearest the centre of mass of the cluster to model the long-range attractive forces between the depositing particles. Otherwise the selection is random.
(6) If a cluster moves, the next step is to allow diffusion within the cluster. This could also be done in all clusters on the surface at this step but this is more computationally time-consuming and so the diffusion of particles in a cluster is considered only when the cluster moves. In practice this makes little difference to the observed patterns. The number of random choices determines the diffusion rate within the cluster and is chosen as $E \times N$, where E is a variable parameter and N is the number of particles in the cluster. Thus the variable parameters in the model are α, R, E and F.

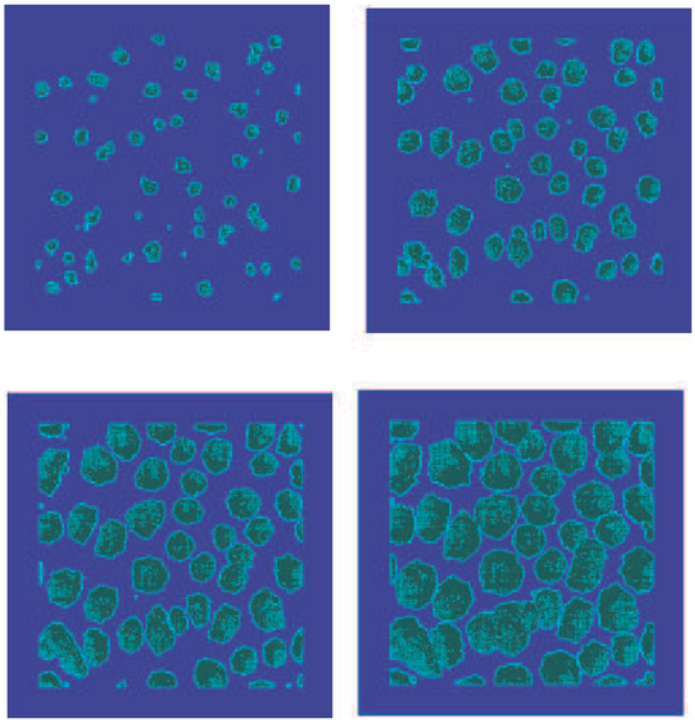

Figure 11. Various stages in the development of thin film growth using the Monte Carlo model showing growth with large-sized islands; $\alpha = 2$, $E = 0.5$, $R = 2$ and $F = 0.0125$.

Thus the basic trial events are (1) landing of a particle or (2) motion of a particle or a cluster followed by motion of particles inside that cluster. The relative proportions between these events is dictated by the physical system. Once these proportions have been decided, the KMC successive steps are chosen at random with probabilities reflecting the selected proportions. However, so far we have not tried to relate the values of these parameters to actual diffusion coefficients or deposition rates. Because the model is at present two-dimensional we cannot say anything yet about three-dimensional growth which depends on the Schoebel barriers for particles moving up and down from terraces. However, the experimental results shown in the next section clearly show that in one case the growth is three-dimensional, whereas the other is not. An improved three-dimensional model, which includes accurate values for these barriers, should be able to capture this effect more accurately.

4.1. Experimental results

Thin fullerite films were grown on glass and mica by thermal evaporation of C_{60} powder. The technique by which the films were evaporated is described in detail in [22]. The image shown in figure 9(a) is of a fullerite film grown on glass and was taken using a scanning force microscope. Figure 9(a) shows clear island structures which are three-dimensional in nature which have distinct boundaries. Such structures indicate a strong preference for the molecules which arrive on the surface to diffuse within the clusters, i.e. large values of E and R. On the other hand, results for mica shown in figure 9(b) indicate two-dimensional patch-like growth on the surface. The growth patterns that develop on mica are stepped flat islands with edges

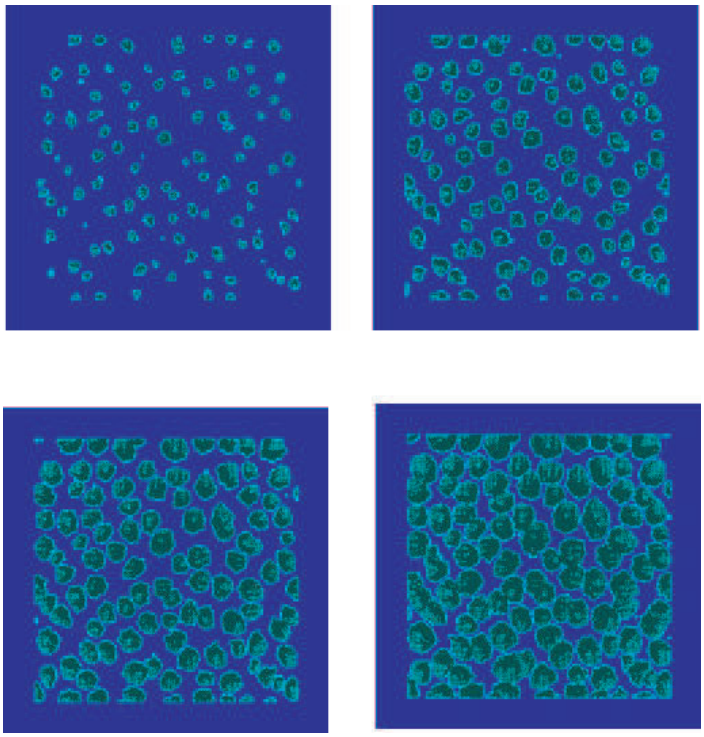

Figure 12. Various stages in the development of thin film growth using the Monte Carlo model showing growth with small-sized islands due to decreased mobility; $\alpha = 4$, $E = 0.5$, $R = 2$ and $F = 0.0125$.

which are not totally convex as in the case of glass. The shapes are not completely fractal in nature, indicating lower values of E and R than in the case of glass.

The fairly simplistic nature of the model means that not all the features of the experimentally observed patterns are captured by the simulation. A more sophisticated approach would be to develop a KMC model based on a proper crystal lattice with transition probabilities determined from energy barriers calculated by either PLATO or classical MD. Such a model involves the determination of all possible transitions which is, in general, still a difficult task and the subject of ongoing research.

4.2. Simulation results

Different sets of parameters are tested and the structures are compared with scanning force images of thin C_{60} films on mica and glass substrates showing different growth modes. If the diffusion radius of particles in the cluster is small, then the growth that develops is of fractal-like clusters whose edges have been smoothed by diffusion. The film coverage patterns for submonolayer coverage are given in figure 10.

This is not completely characteristic of the experimentally observed structures for C_{60} film growth on mica being closer to the structures for gold clusters on ruthenium shown in figure 8. For modelling the growth of C_{60} film on glass the size of the islands that form is regulated by the value of α. For a value of $\alpha = 2$ islands, figure 11, about twice the size form, compared to those shown in figure 12 with $\alpha = 4$. For low surface coverage, a larger α value means

that the islands are less mobile and more numerous because they have not coalesced. They are also smaller in size. Other less symmetric shapes are also possible by suitably varying the parameters.

Since the model does not include a preferred crystalline direction for growth the developing film is characterized only by the number of clusters and the roughness of their edges. However, the model could also be adapted to include the effect of crystallinity. The simulations have demonstrated that for fixed F and E the parameter $\alpha = 1$ controls the number of clusters that form. The shape of the clusters is dependent on E and R and, in the case where there is no diffusion to the centre of mass of a cluster, only by R.

5. Future prospects

With the advent of computers with even faster speeds and more efficient algorithms simulation methods will have an increasing role to play in both explaining and guiding experimental work in this field of nanostructured surfaces. Progress will continue to be made with large systems and longer timescales. In addition, multiscale modelling techniques will also enable many different aspects of a problem to be analysed within a single framework.

Acknowledgments

The authors gratefully acknowledge the input of experimental groups in co-operation with this work; Richard Palmer from Birmingham University, Philip Moriarty from the University of Nottingham and Asta Richter from the University of Applied Sciences, Wildau, Germany. The financial assistance of the NATO Division of Scientific and Environmental Affairs, Collaborative Linkage Grant, PST.CLG.978441 and EC contract IST-1999-11617 are gratefully acknowledged.

References

[1] Smith R 1997 *Atom and Ion Collisions in Solids and at Surfaces* (Cambridge: Cambridge University Press)
[2] Voter A, Montalenti F and Germann T 2002 *Annu. Rev. Mater. Res.* **32** 321
[3] Sanz-Navarro C F and Smith R 2001 *Comput. Phys. Commun.* **177** 206
[4] Betz G and Husinsky W 2002 *Nucl. Instrum. Methods* B **193** 302
[5] Horsfield A P, Kenny S D and Fujitani H 2001 *Phys. Rev.* B **64** 2453
[6] Kenny S D, Horsfield A P and Fujitani H 2000 *Phys. Rev.* B **62** 4899
[7] Smith R and Richter A 1999 *Thin Solid Films* **343** 1
[8] Hartwigsen C, Goedecker S and Hutter J 1998 *Phys. Rev.* B **58** 3641
[9] Goedecker S, Teter M and Hutter J 1996 *Phys. Rev.* B **54** 1703
[10] Smith R, Godwin P D, Kenny S D and Belbruno J 2001 *Surf. Sci.* **490** 409
[11] Godwin P D, Kenny S D and Smith R 2003 *Surf. Sci.* **529** 237
[12] Moriarty P, Ma Y R, Upward M D and Beton P H 1998 *Surf. Sci.* **407** 27
[13] Duffy D M and Blackman J A 1998 *Surf. Sci.* **415** 1016
[14] Guan Ming Wang, Belbruno J, Kenny S D and Smith R 2003 *Surf. Sci.* at press
[15] Hobday S and Smith R 1997 *Faraday Trans.* **93** 3919
[16] Ackland G J, Tichy G, Vitek V and Finnis M W 1987 *Phil. Mag.* A **50** 145
[17] Brenner D W 1990 *Phys. Rev.* B **42** 9458
[18] Brenner D W 1992 *Phys. Rev.* B **46** 1948
[19] Smith R and Beardmore K M 1996 *Thin Solid Films* **272** 255
[20] Rafii-Tabar H, Kamiyama H and Cross M 1997 *Surf. Sci.* **385** 187
[21] Ziegler J F, Biersack J P and Littmark U 1985 *The Stopping and Range of Ions in Solids* (Oxford: Pergamon)
[22] Carroll S J, Nellist P D, Palmer R E, Hobday S and Smith R 2000 *Phys. Rev. Lett.* **84** 2654
[23] Carroll S J, Pratontep S, Streun M, Palmer R E, Hobday S and Smith R 2002 *J. Chem. Phys.* **113** 7723

[24] Steffen H J, Marton D and Rabalais J W 1992 *Phys. Rev. Lett.* **68** 1726
[25] Sanz-Navarro C F 2002 *PhD Thesis* Loughborough University, Loughborough
[26] Kenny D J, Palmer R E, Sanz-Navarro C F and Smith R 2002 *J. Phys.: Condens. Matter* **185** L185
[27] Pratontep S, Preece P, Palmer R E, Sanz-Navarro C F, Kenny S D and Smith R 2000 *Phys. Rev. Lett.* **90** 05503
[28] Sanz-Navarro C F, Smith R, Prantonep S, Kenny D and Palmer R 2001 *Phys. Rev.* B **65** 165420
[29] Pratonep S, Kenny D J, Palmer R E, Sanz-Navarro C F and Smith R 2003 *Phys. Rev. Lett.* **90** 055503
[30] Whitten T A and Sander L M 1981 *Phys. Rev. Lett.* **47** 1400
[31] Hwang R Q, Schroeder J, Guenther C and Behm R J 1991 *Phys. Rev. Lett.* **67** 3279
[32] Richter A and Smith R 2003 *Cryst. Res. Technol.* **38** 250
[33] Richter A, Ries R, Szulzewsky K, Pietzak B and Smith R 1997 *Surf. Sci.* **394** 201